Supporting Information

Atomic-Level Growth Engineering of Si via Acetylene–Silane Co-Deposition for Enhanced Cycle Stability and High Li^+ Dynamics in Si/C Anodes

Xintong Xu [a], Xiao Mu [b], Tao Huang [b]*, Aishui Yu [a,b]*

[a] Department of Chemistry, Collaborative Innovation Center of Chemistry for Energy Materials, Shanghai Key Laboratory of Molecular Catalysis and Innovative Materials, Institute of New Energy, Fudan University, Shanghai 200438, China

[b] College of Smart Materials and Future Energy, Fudan University, Shanghai 200438, China

E-mail: asyu@fudan.edu.cn. (Aishui Yu*)

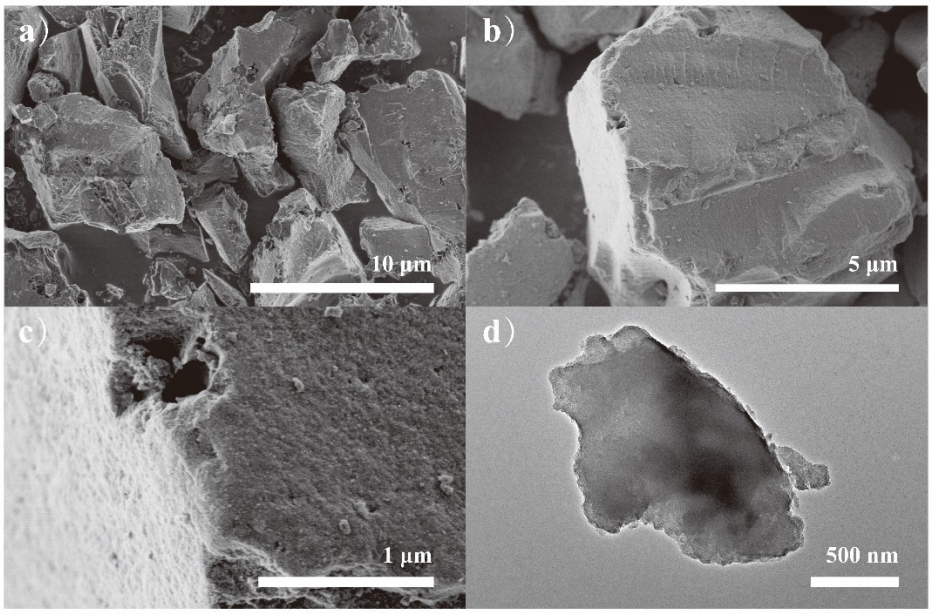

Figure S1 a-c) SEM and d) TEM images of commercial CVD-Si/C.

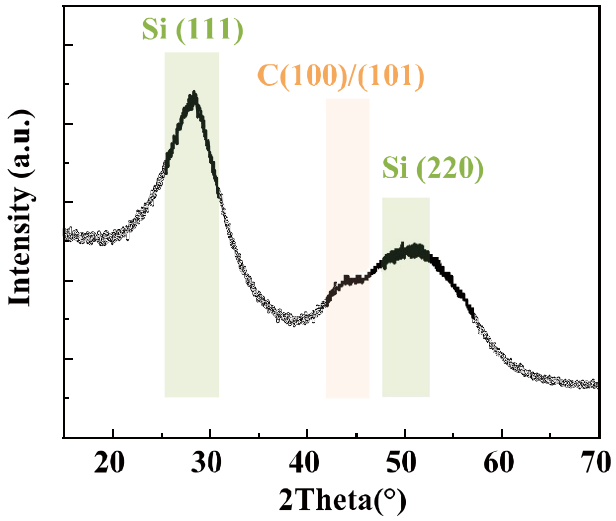

Figure S2 XRD pattern of commercial CVD-Si/C.

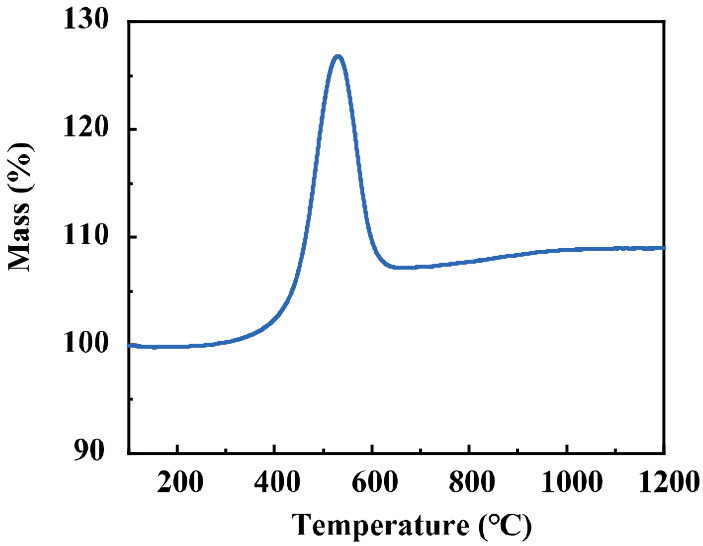

Figure S3 TGA of commercial CVD-Si/C.

Equation S1:

$$w_{Si\ -\ total}\% = \frac{m_2\%}{m_1\%} \times \frac{28}{60}$$

m_1 is defined as the mass percentage of CVD-Si/C measured before oxidation at 100 °C, and m_2 is the mass percentage remaining after oxidation at 1000 °C. The numerical values 28 and 60 represent the atomic mass of silicon and the molar mass of

silicon dioxide (SiO_2), respectively.

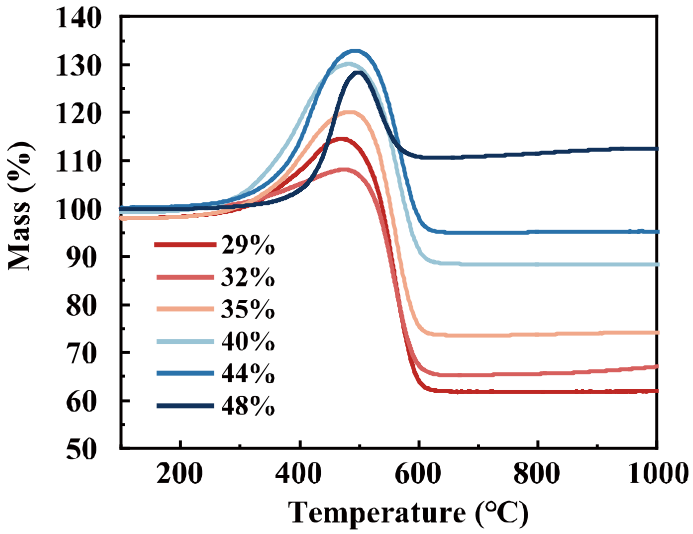

Figure S4 TGA of CVD-Si/C composites with different Si content.

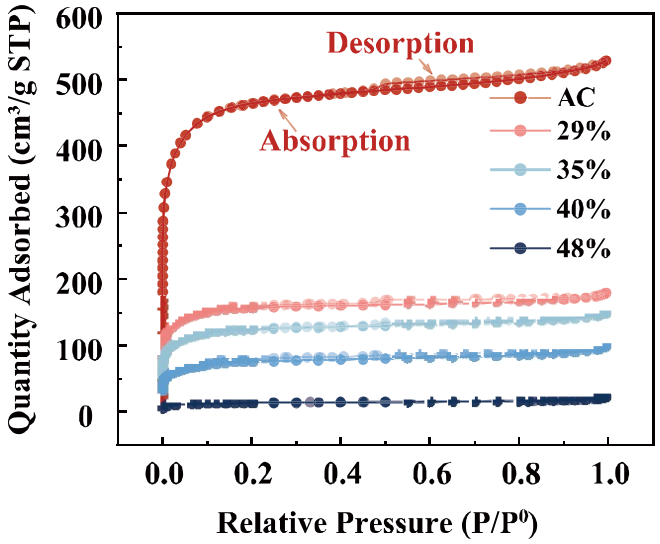

Figure S5 Argon adsorption-desorption analysis on AC and CVD-Si/C samples with different Si content.

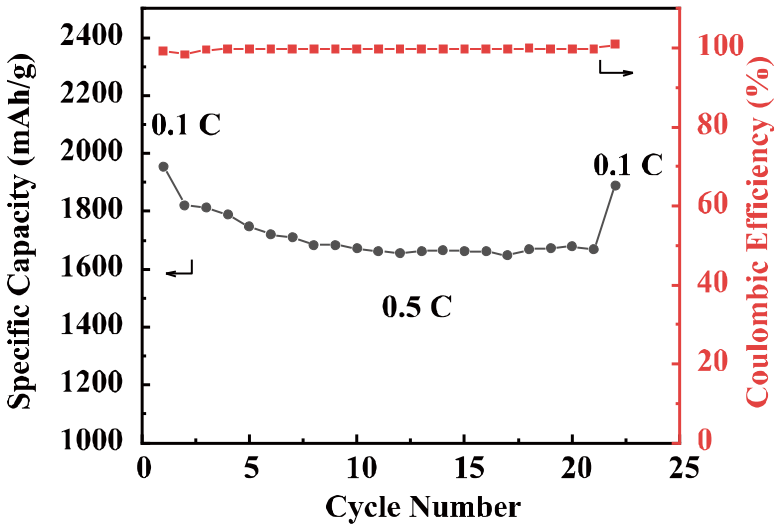

Figure S6 Cycling performance of CVD-Si/C at 0.5C and 0.1C.

Table S1 Summary of reversible capacity, lithium trapping capacity, and SEI-derived capacity loss as a function of silicon content.

Silicon Content (%)	Avg. Reversible Specific Capacity (mAh g^{-1})	CV-Derived Reversible Capacity (mAh g^{-1})	CV Fraction (%)	CE-Derived Irreversible Capacity (mAh g^{-1})	CE Loss Fraction (%)
29	745.94	50.5	7.0	17.2	2.0
32	873.88	46.7	5.5	13.3	1.8
35	1065.26	39.9	3.8	11.2	1.1
40	1174.24	57.0	4.9	14.6	1.2
44	1219.09	70.7	5.8	14.9	1.3

Si Content: Silicon mass fraction in the composite.

Avg. Reversible Specific Capacity: Reversible capacity delivered during galvanostatic cycling.

CV-Derived Reversible Capacity: Reversible capacity released during CV steps, reflecting lithium trapped in Li_xSi.

CV Fraction: Proportion of CV-derived capacity relative to the total reversible capacity.

CE-Derived Irreversible Capacity: Capacity loss attributed to SEI formation, calculated from

coulombic inefficiency.

CE Loss Fraction: Proportion of CE-derived irreversible capacity relative to the total reversible capacity.

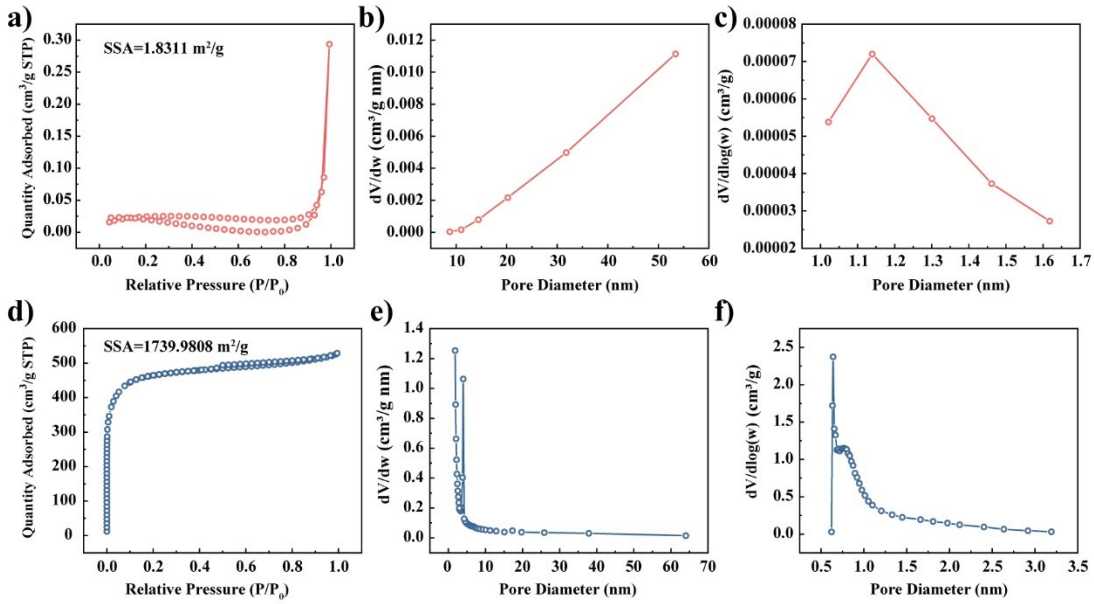

Figure S7 a) Ar adsorption–desorption analysis, b) mesoporous size distribution, and c) micropore size distribution of ACS/SC@C-2. d) Ar adsorption–desorption analysis, e) mesoporous size distribution, and f) micropore size distribution of AC.

Equation S2:

$$w_{Si\text{ - }co\ deposited}\% = \left(\frac{m_3\%}{m_1\%} - 1\right) \times \frac{28}{32}$$

m_1 is defined as the mass percentage of ACS@C or ACS/SC@C measured before oxidation at 100 °C, and m_3 is the mass percentage remaining after oxidation at 400 °C.

Table S2 Detailed TGA data for Si content calculation.

Samples	m_1	m_2	m_3	$w_{Si-co\ deposited}$	$w_{Si-total}$
ACS@C	100.11	86.13	/	/	40.14
ACS/SC@C-1	100.02	81.07	102.36	2.04	38.05
ACS/SC@C-2	100.19	85.22	105.65	4.77	39.54
ACS/SC@C-3	100.56	83.28	107.05	5.65	39.09

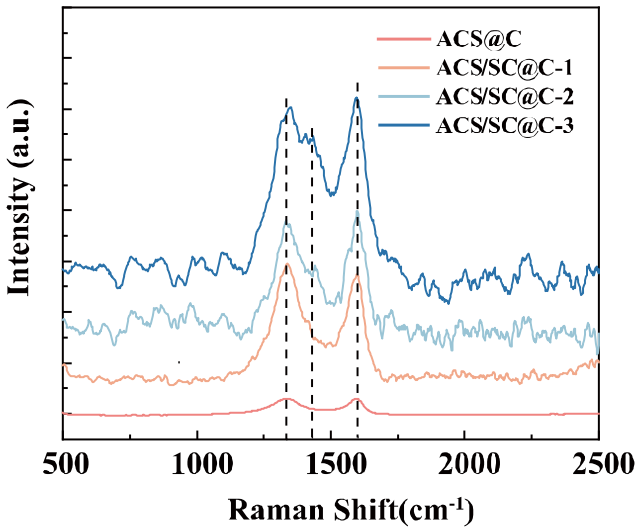

Figure S8 Raman spectroscopy of AC and ACS/SC@C samples.

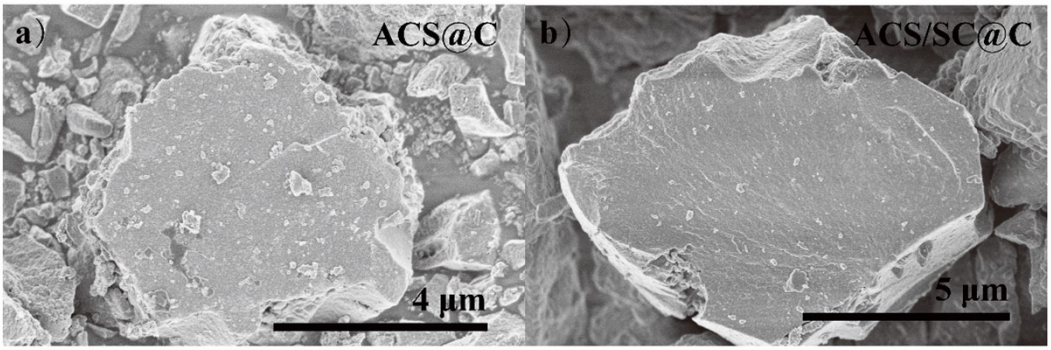

Figure S9 SEM images of a) ACS@C and b) ACS/SC@C.

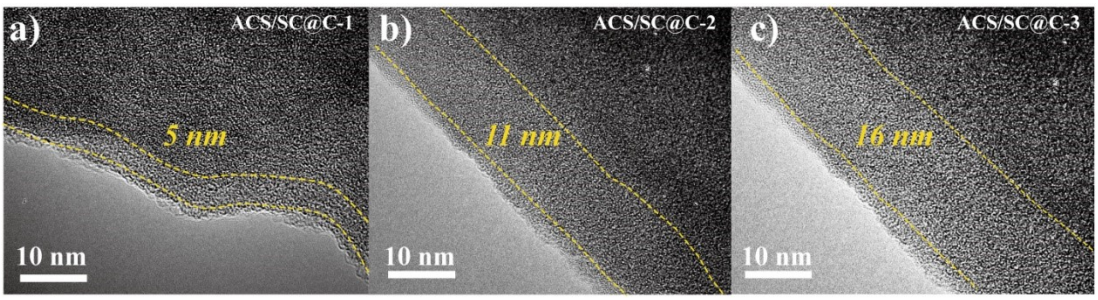

Figure S10 HRTEM images of ACS/SC@C-1, ACS/SC@C-2, and ACS/SC@C-3.

Table S3 Semi-quantitative elemental composition of ACS/SC@C-3 determined by EDS.

Region	C (wt%)	O (wt%)	Si (wt%)
Bulk interior	51.89	5.88	42.23
Co-deposited layer	64.40	6.89	28.71

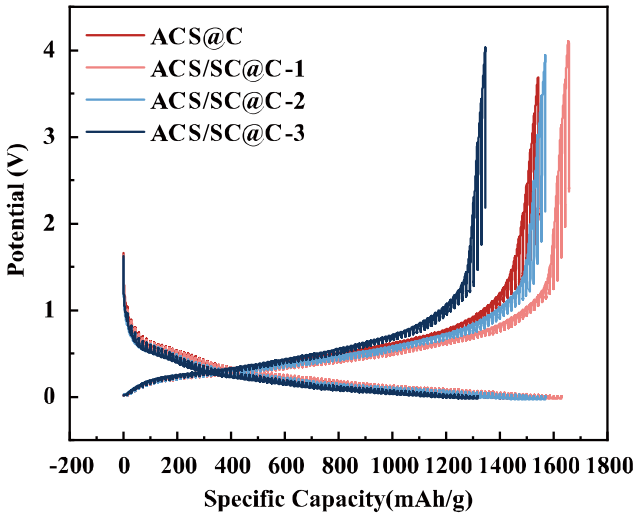

Figure S11 GITT profiles of ACS@C and ACS/SC@C.

Table S4 FTIR peak assignments and corresponding interfacial species during lithiation.

Wavenumber (cm^{-1})	Vibrational Mode	Possible Chemical Species / Origin
1060	ν(P=O) stretching	POF_3 and related phosphate species generated from $LiPF_6$ decomposition
1099	ν(C–O) / ν(C–O–H) stretching	Partially reduced carbonate solvents
1226	ν[(C=O)–O–C] asymmetric stretching (ring-breathing of cyclic carbonates)	Ethylene carbonate (EC) and its early-stage reduction intermediates
1350	$\nu_s(COO^-)$ symmetric stretching	Alkyl lithium carbonates ($ROCO_2Li$) formed in the organic SEI phase
1500	$\nu_{as}(COO^-)$ asymmetric stretching	Lithium carbonate (Li_2CO_3) and related inorganic carbonate SEI components
1755	ν(C=O) stretching of carbonyl groups	Carboxylate-containing intermediates and polymeric organic SEI species
1778, 1809	High-frequency ν(C=O) stretching	Carbonate-based electrolyte solvents (EC, DEC, DMC) and their reactive decomposition intermediates

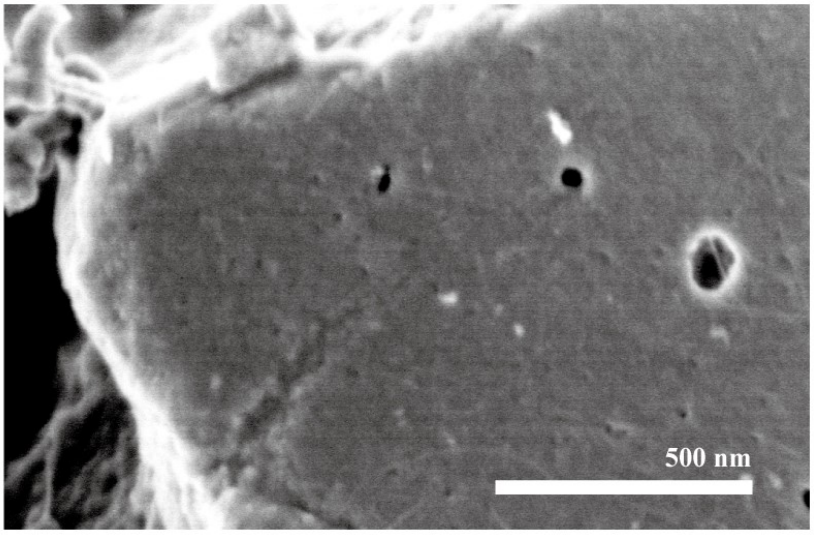

Figure S12 Post-cycling SEM image of the ACS/SC@C electrode after 100 cycles, with the SEI layer removed prior to characterization.

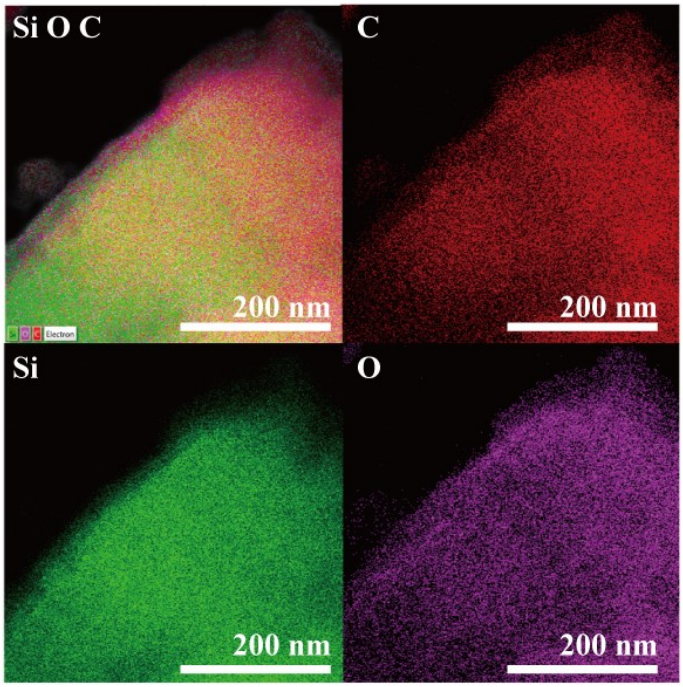

Figure S13 Post-cycling elemental mapping analysis of the ACS/SC@C electrode after 200 cycles.

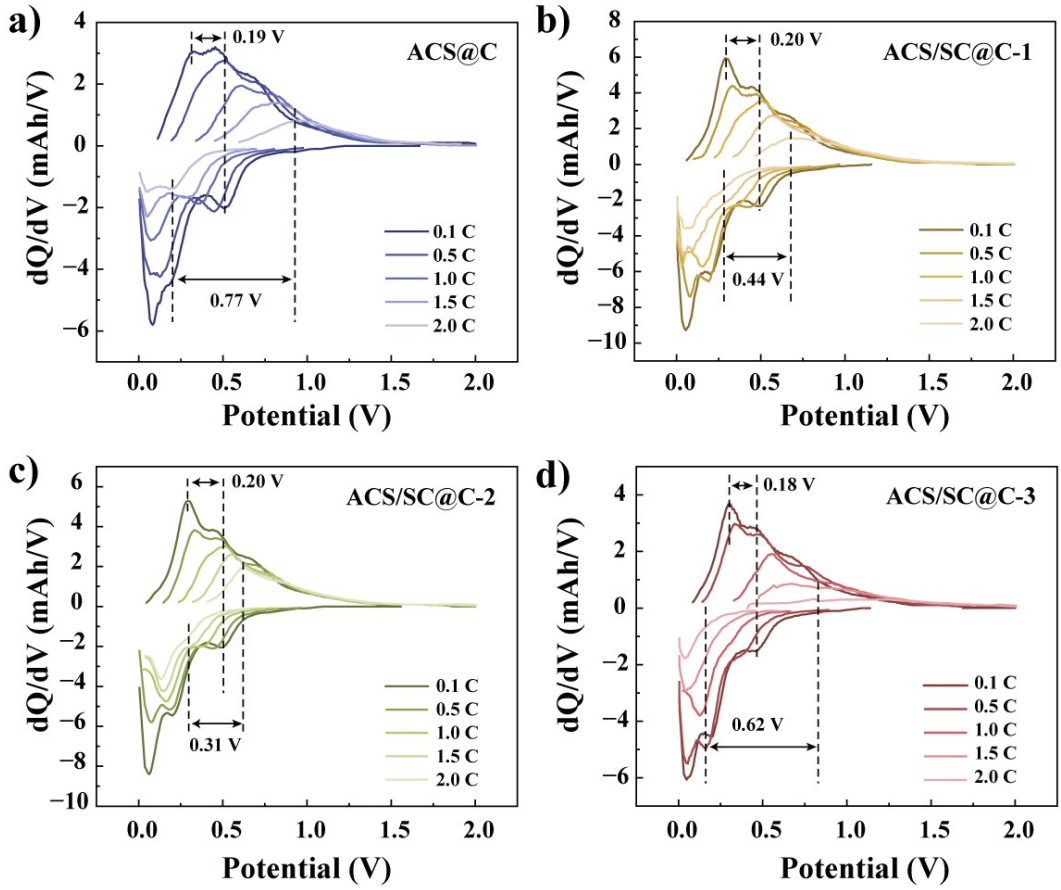

Figure S14 dQ/dV profiles of ACS@C and ACS/SC@C electrodes at different C-rates.

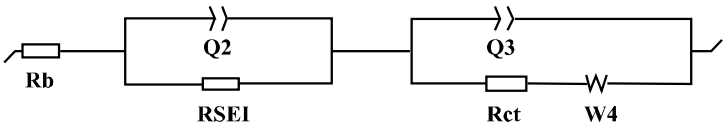

Figure S15 Illustration of the equivalent circuit model.

Table S5 The fitted EIS parameters of ACS@C and ACS/SC@C-2 samples after different cycles.

Sample	Cycle Number	R_b (Ω)	R_{SEI} (Ω)	R_{ct}(Ω)
ACS@C	50	3.869	36.32	58.8
	150	7.962	42.12	219
ACS/SC@C-2	50	4.909	26.74	37.12
	150	3.355	35.35	40.73